Electronic Supplementary Material (ESI) for Analyst.
This journal is © The Royal Society of Chemistry 2024

Towards the Development of a DNA Automaton: Modular RNA-cleaving Deoxyribozyme Logic Gates Regulated by miRNAs

Viktor V. Smirnov, Valerya S. Drozd, Christina K. Patra, Zain Hussein, Daria S. Rybalko, Anastasia V. Kozlova, Moustapha A. Y. Nour, Tatiana P. Zemerova, Olga S.Kolosova, Arseniy Y. Kalnin, Ahmed A. El-Deeb*

Advancements in DNA computation have unlocked molecular-scale information processing possibilities, utilizing the intrinsic properties of DNA for complex logical operations with transformative applications in biomedicine. DNA computation shows promise in molecular diagnostics, enabling precise and sensitive detection of genetic mutations and disease biomarkers. Moreover, it holds potential for targeted gene regulation, facilitating personalized therapeutic interventions with enhanced efficacy and reduced side effects. Herein, we have developed six DNAzyme-based logic gates able to process YES, AND, and NOT Boolean logic. The novelty of this work lies in what we have additionally functionalized them with a common DNA binding strand to the increased cooperativity in input recognition. Moreover, we explored hierarchical input binding to the multi-input logic gates, which helped gate optimization. Additionally, we developed a new design of allosteric hairpin switch used to implement NOT logic. All DNA logic gates achieved the desired true-to-false output signal when detecting a panel of miRNAs, known for their important role in malignancy regulation. This is the first example of DNAzyme-based logic gates having all input-recognizing elements integrated in a single DNA nanostructure, which opens new opportunities in using them for building DNA automatons for diagnosis and therapy of human diseases.

Table of Contents

1. Chemicals and reagents

The oligonucleotides (Table S1, Supplementary materials) were purchased from DNA synthesis (Russia). DNAse/RNAse-free water was purchased from Belbiolab (Russia) and was used for the preparation of all buffers and dilution of lyophilized oligonucleotides. Solid potassium chloride (KCl), sodium chloride (NaCl), and magnesium chloride ($MgCl_2$) we obtained from LenReactive (Russia); and 4-(2-hydroxyethyl)-1-piperazineethanesulfonic acid (HEPES) was purchased from Helicon (Russian) and used as components for the reaction buffer. Urea, Acrylamide, Bisacrylamide, Tris base, Boric acid, and Ethylenediaminetetraacetic acid (EDTA), Ammonium persulfate (APS), Tetramethylethylenediamine (TEMED), were purchased from Helicon (Russia) and used for polyacrylamide gel electrophoresis (PAGE) preparation.

2. Table S1. Oligonucleotides sequences

Table S1. Oligonucleotides used in the study

Name	Sequence 5′ → 3′	ΔG, KJ/mol, Tm, °C
Dza-10n	T[a]CG TCT ATG CTA TGC TAT TGG GCC ATG GTC T AC AAC GA G AGG AAA CCT	-
Dza-9n	TCG TCT ATG CTA TGC TAT TGG GCC ATG GTC T AC AAC GA G AGG AAA CC	-
Dza-8n	TCG TCT ATG CTA TGC TAT TGG GCC ATG GTC T AC AAC GA G AGG AAA C	-
Dzb-9n	GCCCA GGG A GG CTA GCT ATT TTC TCC TAA TGG TGG TCC TAT GGT GGT CAT CTG CT	-
Dzb-8n	CCCA GGG A GG CTA GCT ATT TTC TCC TAA TGG TGG TCC TAT GGT GGT CAT CTG CT	-
Dzb-7n	CCA GGG A GG CTA GCT ATT TTC TCC TAA TGG TGG TCC TAT GGT GGT CAT CTG CT	-
DNA-70	TAG CAG ATG ACC ACC ATA GGA CCA CCA TTA GGA GAA AAT AGA CCA TGG CCC AAT AGC ATA GCA TAG ACG A	-
Parts of logic gates for F_sub		
A parts:		
AK_Dz_a2_sc	CAC AAA CCA TTA ACA ACG A GAG GAA ACC/HEG/[d]TCG TGA GCG C	0.0; 36.4;
VS_OK_Dz_at_sc 3.0	GTTGTTAATGGTTTGTGCTACCTGCACTGTAAGCACTTTG CACAAACCATTA ACAACGA GAGGAAACC /HEG/ TCGTGAGCGC	70.71; 72.1
VS_Dz_at_sc 3.1(ix)	TCGTTGTTACTACCTGCACTGTAAGCACTTTG CACAAACCATTA ACAACGA GAGGAAACC /HEG/ TCGTGAGCGC	-23.85; 53.8;
VS_Dz_at_sc 3.2	GTTGTTAAT CTACCTGCACTGTAAGCACTTTG CACAAACCATTA ACAACGA GAGGAAACC /HEG/ TCGTGAGCGC	-17.57; 49.5;
VS_Dz_at_sc 3.3	TCGTTGTTAATG CTACCTGCACTGTAAGCACTTTG CACAAACCATTA ACAACGA GAGGAAACC /HEG/ TCGTGAGCGC	-40.17; 60.7
VS_Dz_at_sc 3.4	TCGTTGTTAATGGT CTACCTGCACTGTAAGCACTTTG CACAAACCATTA ACAACGA GAGGAAACC /HEG/ TCGTGAGCGC	-51.88; 64.6
VS_Dz at_sc 2.0	AGA AAG GCA GCA GGT CGT ATA G ACG TCT GTT ATG GCT TTC TG ACA AAC CAT TA ACA ACG A GAG GAA ACC /HEG/ TCG TGA GCG C	-31.80; 62.9;
VS_Dz at_sc 2.0.1	AGA AAG GCA GCA GGT CGT ATA G ACG TCT GTT ATGGCT GACA AAC CAT TA ACA ACG A GAG GAA ACC /HEG/ TCG TGA GCG C	-15.90; 55.9;
VS_Dz at_sc 2.0.2	AGA AAG GCA GCA GGT CGT ATA G ACG TCT GTT ATGGCT TT ACA AAC CAT TA ACA ACG A GAG GAA ACC /HEG/ TCG TGA GCG C	-24.27; 60.1;
VS_Dz_at_sc_2.1	CGTCCAGAAAGGCAGCAGGTCGTATAGACGTTGTTAATGGCTTTCTGGACGCAAACCATTAACAACGA GAGGAAACC /HEG/ TCG TGA GCGC	-55.65; 70.1
B parts:		
VS_AK_Dz b_sc	CGA TGA CGG AC /HEG/ CCCAGGGA GG CTA GCT T GTG CTG CTA	-8.37; 51.3;
VS_AK_Dz b_sc(vii)	CGA TGA CGG AC /HEG/ CCAGGGA GG CTA GCT T GTG CTG CTA	-7.53; 57.9;
VS_OK_Dz_bt_sc_1.2(vii)	CGA TGA CGG AC /HEG/ CCAGGGA GG CTA GCT GTG CTG CTA TCA ACA TCA GTC TGA TAA GCT A TAG CAG CAC A	-37.24; 71.5;
VS_VD_Dz_bt_sc_DV1(vii)	CGA TGA CGG AC /HEG/ CCAGGGA GG CTA GCT T GTG CTG CTA TCA ACA TCA GTC TGA TAA GCT A TAG CAG CAC AAGCTAGC	-78.7; 81.9
VS_Dz_bt2_sc 1.3(vii)	CGA TGA CGG AC /HEG/ CCAGGGA GG CTA GCT T GTG CTG CTA TCA ACA TCA GTC TGA TAA GCT A TAG CAG C	-22.60; 64.6;
VS_Dz_bt2_sc 1.4(vii)	CGA TGA CGG AC /HEG/ CCAGGGA GG CTA GCT T GTG CTG CTA TCA ACA TCA GTC TGA TAA GCTATAGCAGCACA AGC	-57.32; 78.8
VS_Dz_bt2_sc 1.5(vii)	CGA TGA CGG AC /HEG/ CCAGGGA GG CTA GCT T GTG CTG CTA TCA ACA TCA GTC TGA TAA GCT A TAG CAG CAC AAGCTAGC CT	-90.80; 86.1
Binding strand:		
AK_Tile_sc 2	GT CCG TCA TCG G CGC TCA CGA	-

Table S1. Continuation of Table 1

Name	Sequence 5′ → 3′	ΔG, KJ/mol, Tm, °C
Parts of logic gate for GFP		
VS,DZa-2i-GFP	CAC AAA CCA TTA ACA ACG A TTC AGG GTC /HEG/TCG TGA GCGC	1.67; 28.2
VS_Dz at_sc-GFP (inhibit)	AGA AAG GCA GCA GGT CGT ATA G ACG TCT GTT ATG GCT TTC TG ACA AAC CAT TA ACA ACG A TTC AGG GTC /HEG/ TCG TGA GCG C	-38.50; 60.8;
VS.Dz_at_sc-GFP: (and)	GTTGTTAATGGTTTGTGCTACCTGCACTGTAAGCACTTTG CACAAACCATTA ACAACGA TTCAGGGTC /HEG/ TCGTGAGCGC	-65.70; 69.3;
VS_Dz b_sc-GFP	CGA TGA CGG AC /HEG/ GTGCAGATGA A GGCTAGCT T GTGCTGCTA	-7.11; 55.9;
VS.DZb-T2- GFP	CGA TGA CGG AC /HEG/ G TGC AGA TGA A GGCTA GCT T GTG CTG CTA TCA ACA TCA GTC TGA TAA GCT A CGG CCC A AGAGAGCCT	-16.74; 54.2;
VS.DZblo-GFP	CGA TGA CGG AC /HEG/ G TGC AGA TGA A GGCTA GCT T GTG CTG CTA TCA ACA TCA GTC TGA TAA GCT A AG CAC A AGAGAGCCT	-40.17; 60.1;
Inputs (miRNAs):		
1st input (hsa-miR-15a-5p)	u[b]ag cag cac aua aug guu ugu g	-
2nd input (hsa-miR-17-5p)	caa agu gcu uac agu gca gg uag	-
3rd input (hsa-miR-21-5p)	uag cuu auc aga cug aug uug a	-
4th input (hsa-let-7d-3p)	cua uac gac cug cug ccu uuc u	-
Substrate:		
F_sub	AAG GTT (FAM)[c] TCC TCg uCCC TGG GCA-BHQ1[e]	-
GFP-60	(FAM) gcc acc uac ggc aag cu g acc cug aag uuc auc ugc acc acc ggc aag cug ccc gug ccc	-

[a] deoxyribonucleotide, [b] ribonucleotide, [c] Fluorescein amidite, [d] Spacer 18 (Hexaethylene glycol), [e] Black Hole Quencher 1.

3. Table S2. Parts of logic gates

Table S2. Parts of logic gates

Name of logic gate	A part	B part
Logic gate for F_sub		
YES	AK_Dz_a2_sc	VS_AK_Dz b_sc(vii)
2iAND-A 1	VS_OK_Dz_at_sc 3.0	VS_AK_Dz b_sc(vii)
2iAND-A 2	VS_Dz_at_sc 3.4	VS_AK_Dz b_sc(vii)
2iAND-A 3	VS_Dz_at_sc 3.3	VS_AK_Dz b_sc(vii)
2iAND-A 4	VS_Dz_at_sc 3.1(ix)	VS_AK_Dz b_sc(vii)
2iAND-A 5	VS_Dz_at_sc 3.2	VS_AK_Dz b_sc(vii)
2iAND-B 1	AK_Dz_a2_sc	VS_Dz_bt2_sc 1.5(vii)
2iAND-B 2	AK_Dz_a2_sc	VS_VD_Dz_bt_sc_DV1(vii)
2iAND-B 3	AK_Dz_a2_sc	VS_Dz_bt2_sc 1.4(vii)
2iAND-B 4	AK_Dz_a2_sc	VS_OK_Dz_bt_sc_1.2(vii)
2iAND-B 5	AK_Dz_a2_sc	VS_Dz_bt2_sc 1.3(vii)
3iAND	VS_Dz_at_sc 3.4	VS_Dz_bt2_sc 1.4(vii)
2iINHIBIT 1	VS_Dz_at_sc_2.1	VS_AK_Dz b_sc(vii)
2iINHIBIT 2	VS_Dz at_sc 2.0	VS_AK_Dz b_sc(vii)
2iINHIBIT 3	VS_Dz at_sc 2.0.2	VS_AK_Dz b_sc(vii)
2iINHIBIT 4	VS_Dz at_sc 2.0.1	VS_AK_Dz b_sc(vii)
3iINHIBIT	VS_Dz at_sc 2.0.2	VS_Dz_bt2_sc 1.4(vii)
Logic gate for GFP		
YES	VS,DZa-2i-GFP	VS_Dz b_sc-GFP
2iAND-A	VS.Dz_at_sc-GFP: (and)	VS_Dz b_sc-GFP
2iAND-B	VS,DZa-2i-GFP	VS.DZblo-GFP
3iAND	VS.Dz_at_sc-GFP: (and)	VS.DZblo-GFP
2iINHIBIT	VS_Dz at_sc-GFP (inhibit)	VS_Dz b_sc-GFP
3iINHIBIT	VS_Dz at_sc-GFP (inhibit)	VS.DZblo-GFP

4. Detailed experimental procedures

4.1 Structure and hybridization prediction

Possible secondary structures formed by DNA oligonucleotides and the corresponding thermodynamic properties were predicted using the DNA folding form of the UNAFold Web Server.[1] Hybridization properties of two oligonucleotides and the corresponding thermodynamic properties were predicted using DINAMelt Web Server, Two State melting (hybridization) tool. Parameters set to: DNA, temperature: 37 °C, concentration of oligonucleotides: 0.1 μM; $[Na^+]$ = 0.165 M, $[Mg^{2+}]$ = 0.002 M, 0.01 or 0.05 M. The tool does not provide a calculation option for a complex of three or more chains, thus, ΔG calculation of multiple strands complex was not possible.

4.2 DNA nanostructures assembling

The annealing process was used for the assembling of DNA nanostructures. The tubes containing an oligonucleotides' mixture of DNA nanostructures' parts (Table S2) (1 μM) and the assembly buffer (150 mM KCl, 15 mM NaCl, 2, 10 or 50 mM $MgCl_2$, 50 mM HEPES, pH – 7,4) were placed in a beaker filled with boiling water, then left to cool down to room temperature overnight.

4.3 Substrate cleavage reaction

F-sub cleavage. The reaction mixture contains F-sub (0.2 μM), cleavage agent (Dz or DNA nanostructure) (0.1 μM), inputs (miRNAs) (0.1 μM or higher in the experiments with INHIBIT gates) and the reaction buffer (150 mM KCl, 15 mM NaCl, 10 or 50 mM $MgCl_2$, 50 mM HEPES, pH – 7,4). The $MgCl_2$ concentrations were selected as relevant based on the former study by Stephen W. Santoro and Gerald F. Joyce, who proposed that a range from 2 mM to 300 mM magnesium concentration rapidly increases the rate of catalysis. Final volume of the reaction mixture was 50 μL. Samples, containing the reaction mixture, were incubated during one hour at 37 °C. Two control samples were added: negative control contained the reaction mixture without cleavage agent, positive control contained 10-23 DNAzyme.

Catalytic activity of DNA logic gates in presence of all input combinations, according to the truth tables, was evaluated by plate fluorometer TECAN Spark (Tecan Nordic AB, Sweden) at the following settings: λ_{ex} = 480 nm, λ_{em} = 525 nm, both slits 10 nm, 30 flashes.

GFP RNA cleavage. GFP RNA substrate was added in final concentration of 1 μM against 0.1 μM of cleavage agents and equimolar concentration of inputs (0.1 μM or higher in experiments with Inhibit gates) in reaction buffer with final value 10 μL. Samples were incubated during 7 or 24 h at 37 °C.

In case of RNA substrate cleavage, a slightly different reaction buffer was used, (150 mM KCl, 15 mM NaCl, 2 mM $MgCl_2$, 50 mM HEPES, pH – 7,4). The transition to 2 mM $MgCl_2$ was made to simulate near physiological conditions for synthetic RNA cleavage.

4.4 Polyacrylamide gel electrophoresis (PAGE)

4.4.1 Assembly of the DNA nanostructures

Native polyacrylamide gel electrophoresis. Mini-PROTEAN® Tetra Handcast Systems (Bio-Rad Laboratories Inc., USA) were used for PAGE. Native polyacrylamide gel composed of 10×TBE solution, 12% of AA:BA solution (acrylamide : bis-acrylamide 29:1, 40% solution), 0.005% of 10% APS solution, and 0.0005% of TEMED, was used for the analysis of DNA logic gates assembly. 3 pmol of each DNA logic gate were analyzed in each lane and 10 (for miRNAs) pmol of each separate composite oligonucleotide were used as control samples. All samples were mixed with 4x loading dye before loading into the gel. Electrophoresis conditions: 80 V, 100 min. Gels were stained with Ethidium bromide and visualized by the ChemiDoc Touch (RT) (Bio-Rad Laboratories, USA).

4.4.2 Cleavage assay of RNA substrate by DNA logic gates

Denaturing polyacrylamide gel electrophoresis. Denaturing polyacrylamide gel composed of 10×TBE solution, 15% of AA:BA solution (acrylamide : bis-acrylamide 29:1, 40% solution), 7 M urea, 0.005% of 10% APS solution, and 0.0005% of TEMED, were used for GFP RNA cleavage testing. Samples were incubated at 95 ºC for 5 min and then placed in ice for 5 min to decompose all intermolecular complexes. After annealing, 8 μl of each sample were loaded into each lane of the gel. Electrophoresis conditions were 80 V, 120 min. The gels were visualized using the ChemiDoc Touch (RT) (Bio-Rad Laboratories, USA). Gels were not stained for visualization, only the 5'-FAM labeled products of the cleavage were visible in the gel.

For the quantitative analysis of the targeted RNA cleavage efficiency the gel images were processed with BioRad Image Lab Software version 6.0.1.

5. Selection optimal a substrate-binding domains for binary Dz

For optimization of the reaction with binary Dz 10-23 for 37 ^{0}C the different combinations of shortened Dz's F-sub binding domains were used with distinct nucleotide length (10-7 nt). In summary it was 9 combinations: Dza-10n/Dzb-9n, Dza-10n/Dzb-8n, Dza-10n/Dzb-7n, Dza-9n/Dzb-9n, Dza-9n/Dzb-8n, Dza-9n/Dzb-7n, Dza-8n/Dzb-9n, Dza-8n/Dzb-8n, Dza-8n/Dzb-7n. The DNAzyme's arms were taken in the reaction in concentrations 5 nM of Dza and 20 nM of Dzb. F-sub were taken in concentration of 200 nM. DNA-70 (the synthetic model fragment of ssDNA) was taken as the analyte in concentration of 1 nM. The incubation was provided in a water bath with a temperature of 37 ^{0}C for 1 h. After incubation the fluorescence reading was provided on a Tecan on the wavelengths of 480 nm (Ex) and 525 nm (Em). In later work the combination of shortened DNAzyme arms with the best fluorescent signal was chosen. Based on our results it was Dza-9n/Dzb-7n (Figure S1A).

The YES was designed in the beginning and became the basis for all subsequent logic gates. The YES was designed with the lengths of the substrate-binding domains (Dza-9n and Dzb-7n) and produces 80% of the signal compared to Dz (Figure S1B). The YES showing greater intensity became the basis for our subsequent designs.

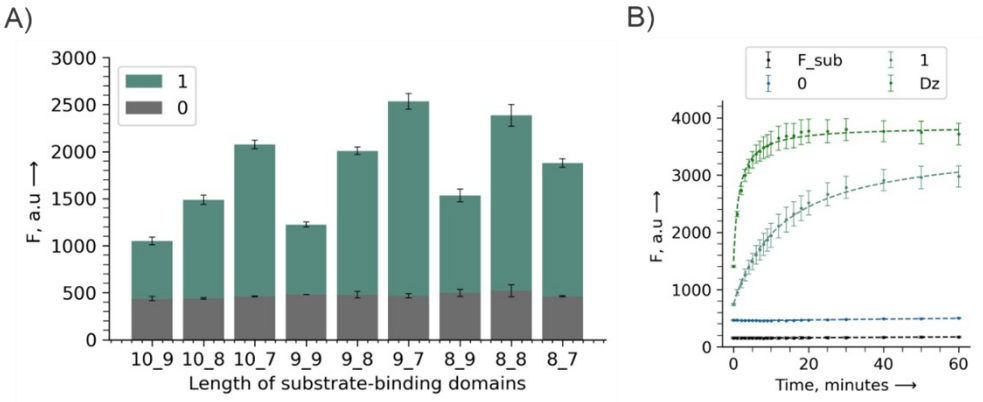

Figure S1. The fluorescence intensity by A) binary Dz with different length of F_sub binding domains and C) Fluorescence curve of YES gate processing

6. Optimization of incubation time

The optimal incubation time for comparing performing signals by logic gates and signal by 10-23 Dz was chosen as 1 h. This condition is necessary to evaluate the efficiency of logic gates compared to Dz, its catalytic core sequence being the basis of all logic gates. A variable time incubation experiment with Dz showed that the intensity plateau after 1 hour (Figure S2).

In addition, the incubation time chosen to evaluate the efficiencies of the logic gates and the 10-23 Dz signals was set to less than 1 minute. This time frame is considered sufficient for a preliminary evaluation of the relative efficiencies of the logic gates derived from Dz. The rationale for this choice is based on the observation that within this short incubation period, substrate cleavage exhibits a linear progression that directly correlates with reaction rate. While a comprehensive analysis involving the determination of Michaelis constants and maximum reaction rates would provide a more in-depth understanding, the current approach provides a simplified yet effective method for this comparative study.

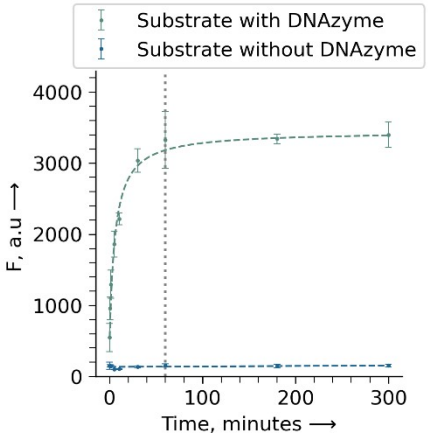

Figure S2. Graph of fluorescence intensity of F_sub cleaved by Dz

7. DNA binding strand design

A DNA binding strand was designed that holds two pieces of DNA logic gates side by side. The DNA sequence 21 nt long is shown in Table S1 with the name AK_Tile_sc 2. The DNA binding strand meets two important conditions: (i) Not to have off-target hybridization with all oligonucleotides from the study. (ii) The melting temperature of the duplexes between the binding strand and the DNA logic gate domains binding to the DNA strand must be your than the reaction temperature (37 °C).

Fulfillment of the first condition. A table with calculated parameters using Mfold (Parameters set to: DNA, temperature: 37 °C, concentration of oligonucleotides: 0.1 µM; $[Na^+]$ = 0.165 M, $[Mg^{2+}]$ = 0.01 M.) was made, which shows that the DNA binding stand does not form stable duplexes in oligonucleotides. Hybridization of DNA binding strand with identical sites in VS_Dz b_sc-GFP, VS.DZb-T2- GFP, VS.DZbloGFP, (ΔG=-33.5 KJ/mol, Tm=26.0°C) is possible. However, these sites fold into hairpins with Tm=48.0...63.2°C. Therefore, the hairpin state will predominate in solution and no interference due to off-target hybridization is expected.

Table S3. Calculated parameters of hybridization of DNA binding strand with oligonucleotides from the study. For calculations, oligonucleotides have the binding domains removed.

Name of oligonucleotide	ΔG, KJ/mol	Tm, °C	Name of oligonucleotide	ΔG, KJ/mol	Tm, °C
AK_Dz_a2_sc	-19.7	1.6	VS_Dz_bt2_sc 1.4(vii)	-15.1	< 0
VS_OK_Dz_at_sc 3.0	-19.7	1.6	VS_Dz_bt2_sc 1.5(vii)	-15.1	< 0
VS_Dz_at_sc 3.1(ix)	-19.7	1.6	VS,DZa-2i-GFP	-16.7	< 0
VS_Dz_at_sc 3.2	-19.7	1.6	VS_Dz at_sc-GFP	-20.1	1.0
VS_Dz_at_sc 3.3	-15.5	< 0	VS.Dz_at_sc-GFP	-16.7	< 0
VS_Dz_at_sc 3.4	-19.7	1.6	VS_Dz b_sc-GFP	-33.5	26.0
VS_Dz at_sc 2.0	-20.1	1.0	VS.DZb-T2- GFP	-33.5	26.0
VS_Dz at_sc 2.0.1	-20.1	1.0	VS.DZblo-GFP	-33.5	26.0
VS_Dz at_sc 2.0.2	-20.1	1.0	1st input	-15.1	< 0
VS_Dz_at_sc_2.1	-20.1	1.0	2nd input	-17.2	< 0
VS_AK_Dz b_sc	-14.6	< 0	3rd input	-16.7	< 0
VS_AK_Dz b_sc(vii)	-14.6	< 0	4th input	-16.7	4.0
VS_OK_Dz_bt_sc_1.2(vi)	-15.1	< 0	F_sub	-14.2	< 0
VS_VD_Dz_bt_sc_DV1(vii)	-15.1	< 0	GFP-60	-20.9	< 0
VS_Dz_bt2_sc 1.3(vii)	-14.6	< 0	AK_Tile_sc 2	-25.1	13.7

Fulfillment of the second condition. Figure S3 shows the predicted secondary structure of YES gate using Nupack (Parameters set to: DNA, temperature: 37 °C, concentration of oligonucleotides: 0.1 µM; $[Na^+]$ = 0.165 M, $[Mg^{2+}]$ = 0.01 M). The melting temperatures of duplexes formed by DNA binding strand and binding domains (-47.9°C and -44.6°C) are higher than the reaction temperature (37°C), hence it is expected that a stable complex will be formed, which is confirmed by the observations in the figure S5 and S9.

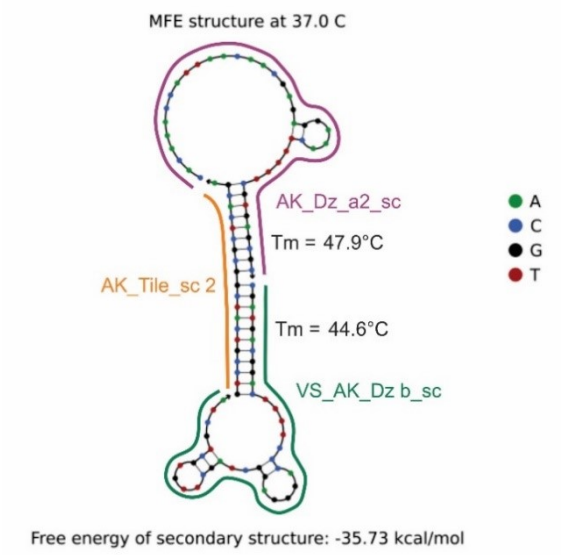

Figure S3. Predicted secondary structure of YES gate using Nupack. Oligonucleotides are marked with different colors, "HEG" linkers are replaced by "TTT", calculated melting point of duplexes using Mfold is shown

8. GFP-60 design

In our study, we used a synthetic mRNA fragment of GFP as substrate. This specific fragment was selected through a two-step selection process, and its utility was confirmed by a knockdown experiment using an antisense oligonucleotide (these data are not included). It is noteworthy that the same mRNA fragment was also used in Drozd's research.[2]
The selection process for the target fragment was meticulous and involved two stages:

1. Initially, we identified 33 GU sites within the mRNA sequence, as these sites are known to be optimally cleaved by the 10-23 Dz.
2. Subsequently, we conducted an analysis of the local stability of RNA fragments containing these cleavage sites. This analysis was performed using the Mfold service,[1] providing insights into the structural aspects that influence the cleavage efficiency.

The selected fragments of 60 nt trusted fragments had one of the lowest folding energies of -13.4 kcal/mol out of all fragments tested. Moreover, the folding of the separate fragment was identical to its folding in the context of the full-length GFP mRNA. This selection procedure suggests the selected fragment can be accessible by oligonucleotide gene therapy agents in living cells.
To verify this we designed and tested an antisense oligonucleotide (ASO) against this fragment as well as against other two fragments in the same mRNA. It was found that GFP fluorescence was suppressed most efficiently in cell culture using the ASO against the fragment reported in this study (data not shown). This data indicates that the chosen site is a promising target for the DNA logic gates reported in this study.

9. The cooperative performance of Dza and Dzb

With diffusing Dza, Dzb, the reaction may be slower due to the need for random collision of all components. And when Dza and Dzb are localized on the DNA binding strand, the reaction may be faster because the constant proximity of the enzyme halves simplifies the process of their interaction and active site formation. In this system, the Dz halves are fixed, Dz can cleave the substrate faster. This is because fixation of the halves reduces the "search time" for their interaction, increasing the probability of formation of the Dz active site.
On these assumptions, it is expected that if DNA binding strand is added, catalytic activity will increase due to spatial localization. This would result in a high percentage of substrate cleavage and a decrease in the concentration input required for appreciable substrate cleavage.
We will consider two bound states, when the BiDZ is bound to the tile and when it is unbound. We will review two of articles, in which we used similar DNA systems. In his study, Gomes de Oliveira conducted experiments with BiDz parts that were freely diffusing.[3] In contrast, Christina Patra's research involved experimentation on a DNA nanomachine, where BiDz parts were attached to tiles.[4] The two articles used the same reaction conditions and same DNA sequences. Therefore, we can compare them to see if there is a significant difference with/without tile attaching.
We can verify that the BiDZ parts are assembled on the tile by the bands above the 90 nt label in lanes 3, 4, and 5 in Figure S3 - Long RNA-46 targeting Threshold DNA-nanomachines assembly in 12% native PAGE.[4]
The reaction conditions in the two articles are the same and are summarized in table S4.

Table S4. Buffer and reaction condition for RNA-46 cleavage assay.

	BiDz (Without tile, diffusing)	DNA-nanomachine (With tile, localized)
Buffer:		
HEPES, mM	50	50
pH	7.5	7.4
KCl, mM	150	150
NaCl, mM	15	15
$MgCl_2$, mM	2	2
Reaction condition:		
RNA-46, uM	1	1
miR-17, nM	25…300	25…1000
DNA machine, nm	100	100
Temperature, ^0C	37	37
Time incubation, h	24	24

The sequences used in the two studies are also the same except for the parts for tile attachment in Table S5.

Table S5. Oligonucleotide sequences used for assembly of RNA-46

BiDz (Without tile, diffusing)		DNA-nanomachine (With tile, localized)	
RNA-46	gua cuu gag cuc cac ucc gca gcg ucu gaa guu gcu gga cgc gua c	RNA-46	gua cuu gag cuc cac ucc gca gcg ucu gaa guu gcu gga cgc gua c
RNA_miR-17 5	caa agu gcu uac agu gca ggu ag	hsa-miR-17-5p RNA	caa agu gcu uac agu gca ggu ag
RDza-46	CTA CCT GCA CTG ACA ACG A GCT GCG GAG	T1-DZa-46	CTA CCT GCA CTG ACA ACG A GCT GCG GAG /HEG/ CAC ACG TGT TCT GTT CAT CTA
RDzb-46	GCA ACT TCA G AGG CTA GCT TAA GCA CTT TG	T2-DZb-46	GTG TGC ACA ACA CAA GTG GAT /HEG/ GCA ACT TCA G A GG CTA GCT TAA GCA CTT TG
RDza-46-Th	AGG TAG CTA CCT GCA CTG TAA GCA CTT TG CTA CCT GCA CTG ACA ACG A GCT GCG GAG	T1-DZa-Th-46	AGG TAG CTA CCT GCA CTG TAA GCA CTT TG CTA CCT GCA CTG ACA ACG A GCT GCG GAG /HEG/ CAC ACG TGT TCT GTT CAT CTA
RDzb-46-Th	GCA ACT TCA G AGG CTA GCT TAA GCA CTT TG CTA CCT GCA CTG TAA GCA CTT TG CAA AGT GCT TA	T2-DZb-Th-46	GTG TGC ACA ACA CAA GTG GAT /HEG/ GCA ACT TCA G AGG CTA GCT TAA GCA CTT TG CTA CCT GCA CTG TAA GCA CTT TG CAA AGT GCT TA

The results from the two studies are presented in table S6.

Table S6 Results comparison

	BiDz (Without tile, diffusing) Data from Figure S6C[3]			DNA-nanomachine (With tile, localized) Data from Figure 2D[4]		
	BiRDz-46	DTh-2i-46	DTh-3i-46	DNM-yes-46	DNM-2i-46	DNM-3i-46
Min. concentration activation, nM [a]	5	50	142	2	25	55
Concentration of max cleavage, nM	100	200	300	100	200	300
Max RNA-46 cleavage, %	31	35	35	~85	~90	~95

[a] The minimum concentration when percentage cleavage more than 3 standard deviation above background average (The activation threshold).

Table S6 shows that the DNA-nanomachine showed a decrease in the threshold activation by about 2-fold and an increase in RNA cleavage by more than 55%. Accordingly, this fulfills our expectation that BiDz localization increases substrate cleavage efficiency.

10. Designing optimization and assembly of two 2iAND

Our observations demonstrate that the optimal parameter values for parts A and B do not coincide, which would seem to indicate the distinct interactions with different miRNAs, which form complexes with varying stabilities. Specifically, the 1st input exhibits a stronger interaction with part A (ΔG = -49.8 kJ/mol) compared to part B (ΔG = -47.3 kJ/mol). Furthermore, the complex formed between 2nd input and part A is more stable (ΔG = -113.0 kJ/mol) than the complex formed between 3rd input and part B (ΔG = -98.3 kJ/mol). These findings explain a shift of the optimal parameter region towards the more stable complex, underscoring the importance of the stability of the miRNA-part interaction in the design of highly efficient AND gates.
The activity of 2iAND-A and 2iAND-B with different combinations of input signals as a function of time is demonstrated in Figure 1A and 1C. The minimum time and time interval of the high ratio between the true and false signal for both best 2iAND were determined. The 2iAND-A gate produces a positive signal that is twice the false signal within 2 minutes of initiating the reaction. Furthermore, during the interval 7-50 min, the ratio between the true and false signal is maintained over 3.0±0.3 (Figure S3B). The 2iAND-B gate produces a positive signal that is twice the false signal in 2 minutes and the interval between 5 min and 14 min is maintained over 2.3±0.8 (Figure S4D). At 25 and 8 minutes, the AND gates give the maximum value of the ratio 3.4±0.6 and 2.4±0.8 of true and false signals for 2iAND-A and 2iAND-B, respectively.

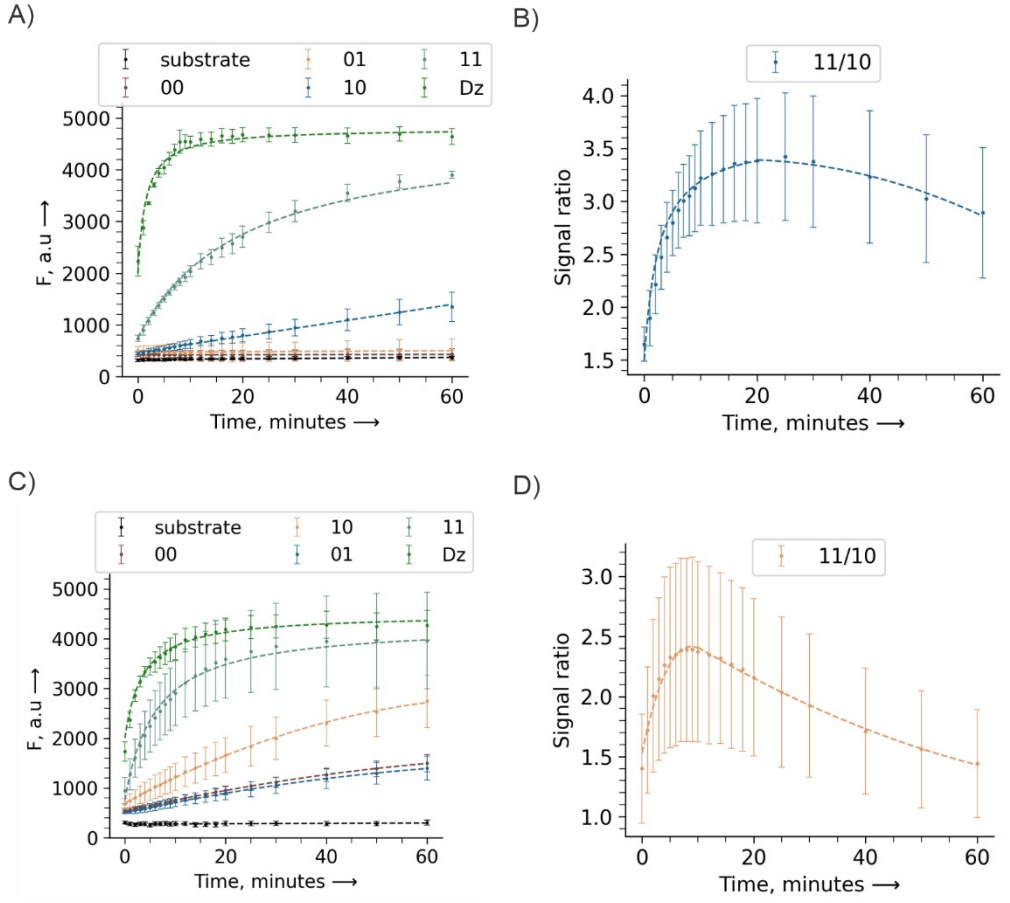

Figure S4. The horizontal axis represents the time reaction, while the vertical axis represents: A) and C) the fluorescence intensity of F_sub; B) and D) the ratio of fluorescence intensity between true and false signals. Temperature incubation: 37 °C, concentration of oligonucleotides: 0.1 μM; [Na^+] = 0.165 M, [Mg^{2+}] = 0.01 M.

Using gel electrophoresis, we were able to elucidate the underlying mechanism of the AND gates (Figure S5). Lane 1-4 have assembled AND gates above the level of 100 nt. In lane 3 with additional 1st input there are upper bands. Apparently, 1st input binds with AND gate. Also, in lane 4 there is a light upper band, 3rd input binds with the complex AND gate. The complex of AND gate with both inputs is not stable for the PAGE analysis. Probably, associating the complex with both inputs is a dynamic process in solution. Bands in lanes 5-7 are parts of AND gate. Specifically, the gates operate through a sequential process in which input interacts with the folded strand and triggers the unfolding of the hairpin. The unfolded strand then serves as a platform for the input to bind and form a catalytic core, thereby enabling the subsequent cleavage of the substrate.

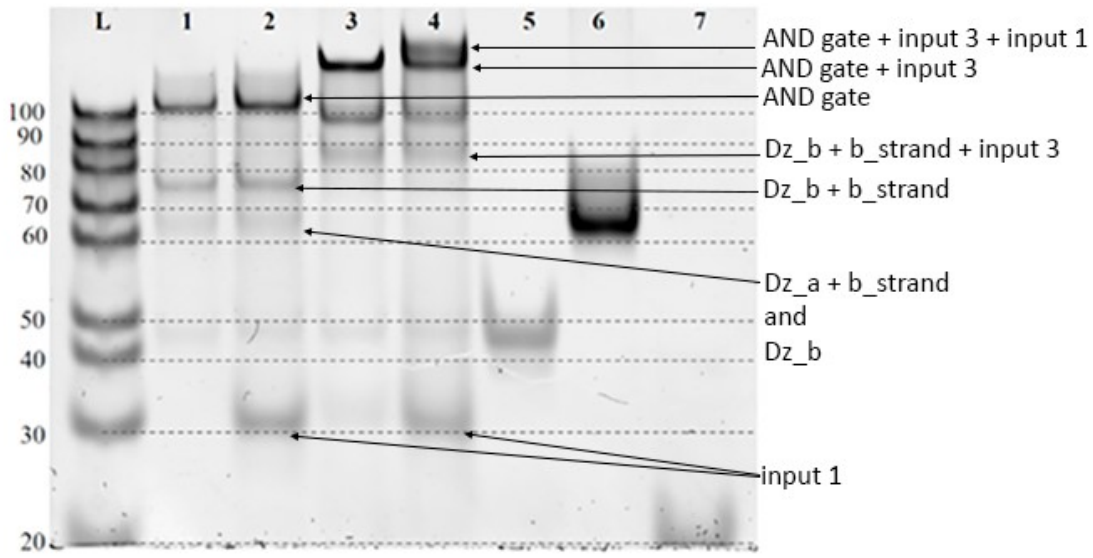

Figure S5. PAGE analysis of the interaction of 2iAND-B with inputs. L - Ladder 20-100 nt (single stranded DNA); 1 - AND; 2 - AND with 1st input; 3 - AND with 3rd input; 4 - AND with both inputs; 5 - Dz_a; 6 - Dz_b; 7 – DNA binding strand (b_strand)

11. Designing a 3iAND

Moreover, the 3iAND (with three input strands) was assembled from optimal 2iAND gates due to the interchangeable modular design (Figure 1D). The 3iAND produces a positive signal at the interval between 4 min and 16 min is maintained over 1.68±0.04. At 7 minutes, the 3iAND gates produce the maximum value for the ratio 1.87±0.05 of true to false signals (Figure S6B).

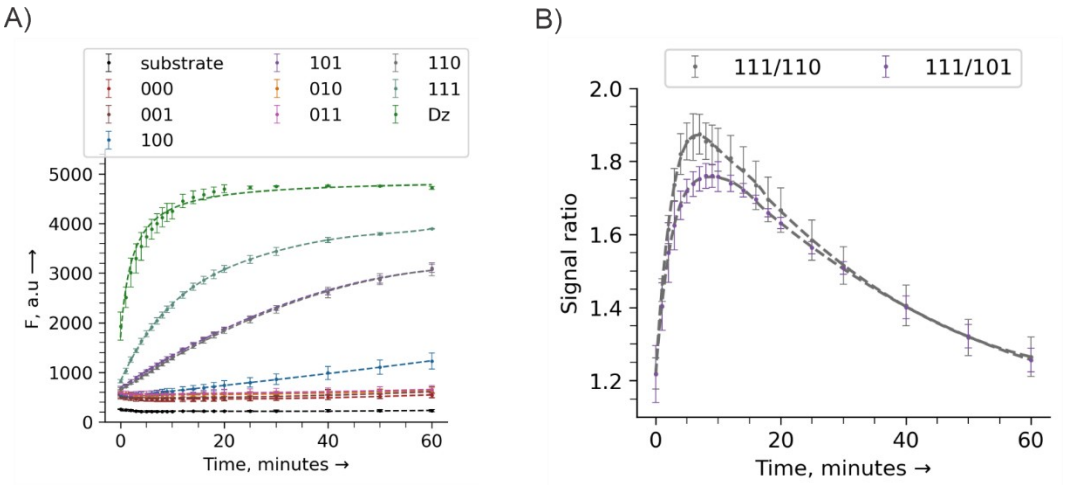

Figure S6. The horizontal axis represents the time reaction, while the vertical axis represents: (A) the fluorescence intensity of F_sub; (B) the ratio of fluorescence intensity between true and false signals. Temperature incubation: 37 °C, concentration of oligonucleotides: 0.1 μM; [Na^+] = 0.165 M, [Mg^{2+}] = 0.01 M

12. Designing a 2iINHIBIT, 3iINHIBIT. Assembly 2iINHIBIT gate

The optimal design demonstrated a reduction in fluorescent signal only by 27% compared to Dz, while inhibiting a signal by 55%, using a 1x miR-let-7d concentration and 94% using 2x one (Figure S7). The correct signal is produced in the interval 2 min to 8 min with 1x miR-let-7d. The ratio between the true and false signal (10/11) is maintained over 1.69±0.12. The correct signal with 2x miR-let-7d is observed at all times (Figure S8A). In particular, the interval 20-60 min, the ratio 10/11x2 is maintained over 5.11±0.2 (Figure S8B).

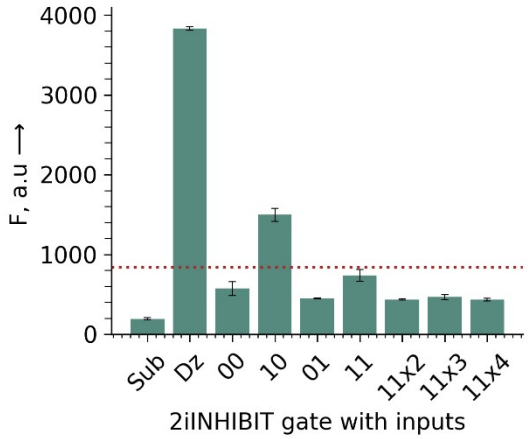

Figure S7. Fluorescence intensity by the optimized 2iINHIBIT gate for inputs during 1 h incubation

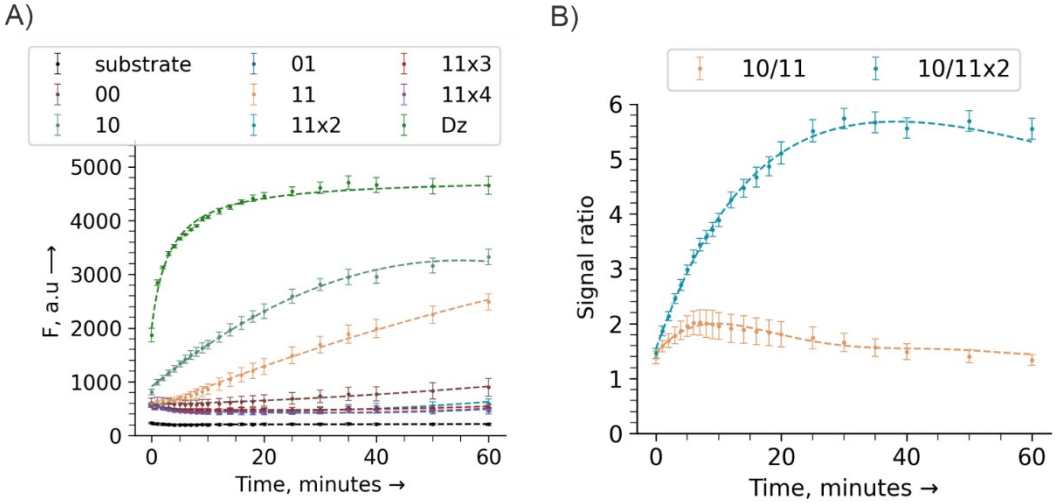

Figure S8. The horizontal axis represents the time reaction, while the vertical axis represents: A) the fluorescence intensity of F_sub; B) the ratio of fluorescence intensity between true and false signals. Temperature incubation: 37 °C, concentration of oligonucleotides: 0.1 μM; $[Na^+]$ = 0.165 M, $[Mg^{2+}]$ = 0.01 M

In Figure S9 the lane 1-2 has an INHIBIT above the level of 100 nt. In lane 2 the complex of INHIBIT with 1st input looks like a slight band. It is not stable for the PAGE analysis. In lane 3 the highest band is the complex of INHIBIT with 4th input. In lanes 3-7 the band of INHIBIT is absent, meaning that a major amount of INHIBIT binds with 4th input. In lanes 5-7 there is a band between 40-50 nt. level, it's an excessive amount of 4th input. Lanes 8-12 are parts of the INHIBIT.

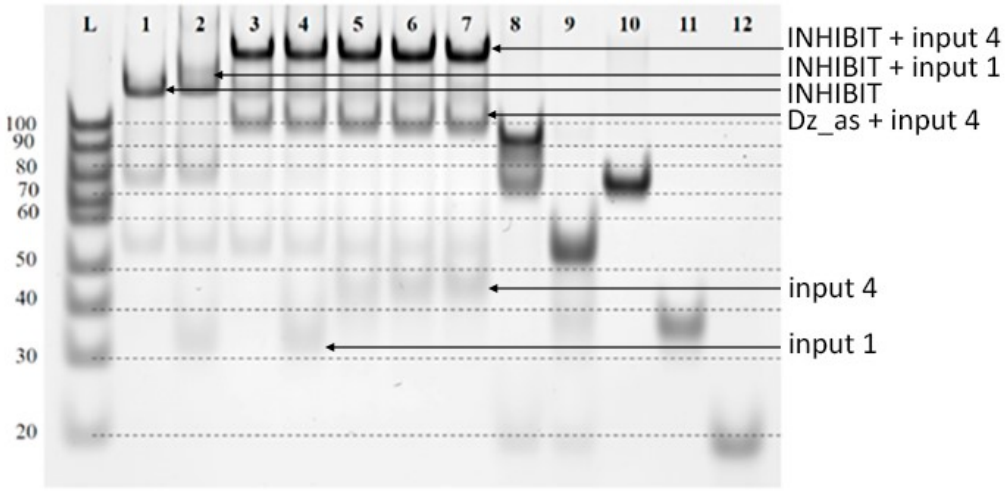

Figure S9. PAGE analysis of the interaction of 2iINHIBIT with inputs. L - Ladder 20-100 nt (single stranded DNA); 1 - INHIBIT; 2 - INHIBIT with 1st input; 3 - INHIBIT with 4th input; 4-7 INHIBIT with both inputs where 4th input has concentration 100-400 nM; 8 - Dz_as with b_strand; 9 - Dz_b with b_strand; 10 - Dz_a; 11 - Dz_b; 12 – b_strand

Using the modular structure approach, we successfully constructed the 3iINHIBIT gate, as depicted in Figure 3F. The 3iINHIBIT generated a correct positive signal with 1x miR-let-7d in the interval 1-30 minutes. The correct signal with 2x miR-let-7d is observed at all times (Figure S10B).

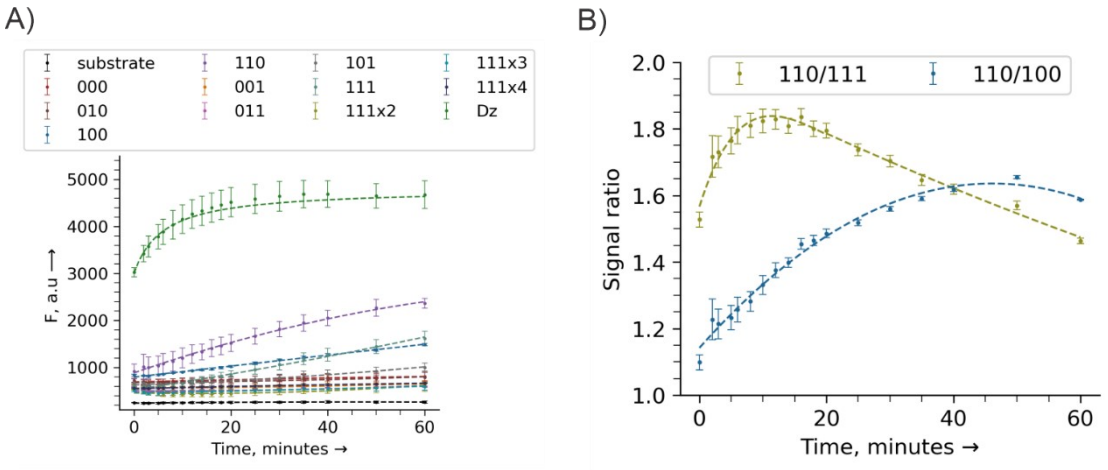

Figure S10. The horizontal axis represents the time reaction, while the vertical axis represents: A) the fluorescence intensity of F_sub; B) the ratio of fluorescence intensity between true and false signals. Temperature incubation: 37 °C, concentration of oligonucleotides: 0.1 µM; [Na^+] = 0.165 M, [Mg^{2+}] = 0.01 M.

13. Designing logic gates for RNA substrate

All logic gates produced the correct output signal. For YES and 2iAND, a correct signal differentiated from the background was observed after only 7 hours (Figure S11). 3iAND, and INHIBIT required 24 hours of incubation (Figure S12).

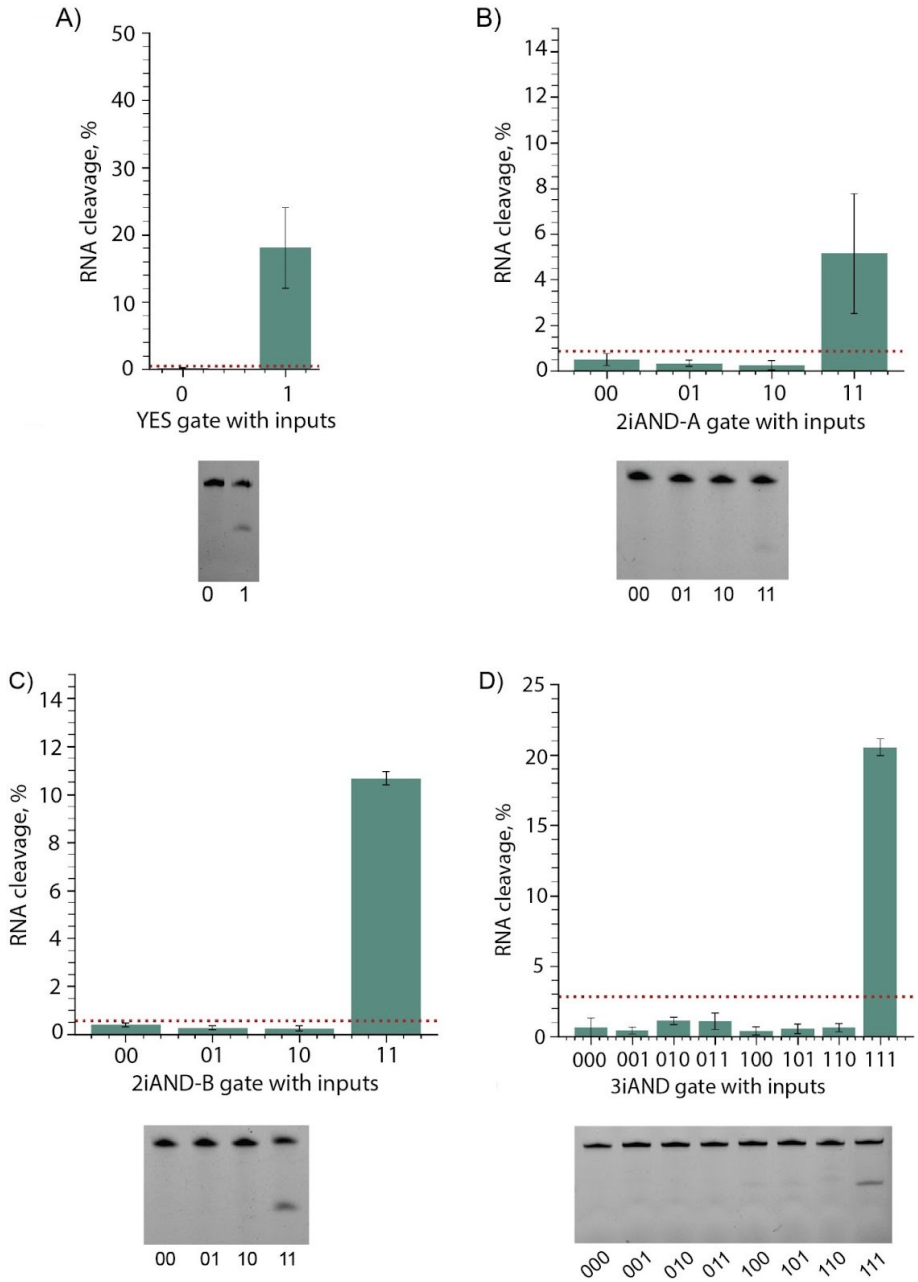

Figure S11. Cleavage RNA by AND gates for inputs after incubation: (A-C) 7 h; (D) 24 h. Temperature incubation: 37 °C, concentration of oligonucleotides: 0.1 μM; $[Na^+]$ = 0.165 M, $[Mg^{2+}]$ = 0.002 M.

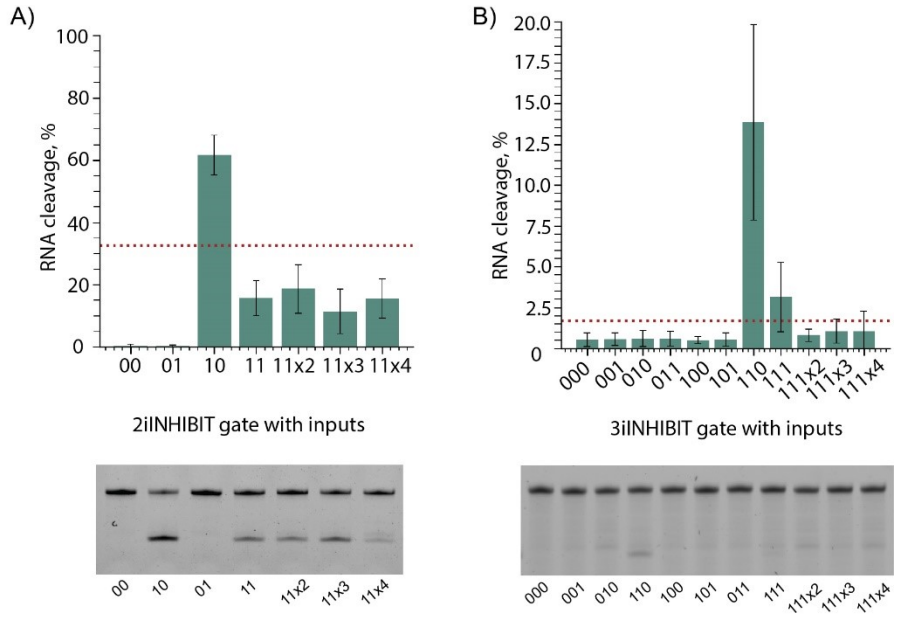

Figure S12. Cleavage RNA by INHIBIT gates for inputs after incubation 24 h. Temperature incubation: 37 °C, concentration of oligonucleotides: 0.1 µM; [Na^+] = 0.165 M, [Mg^{2+}] = 0.002 M.

14. Schematic of 2iINHIBIT and 3iINHIBIT gates

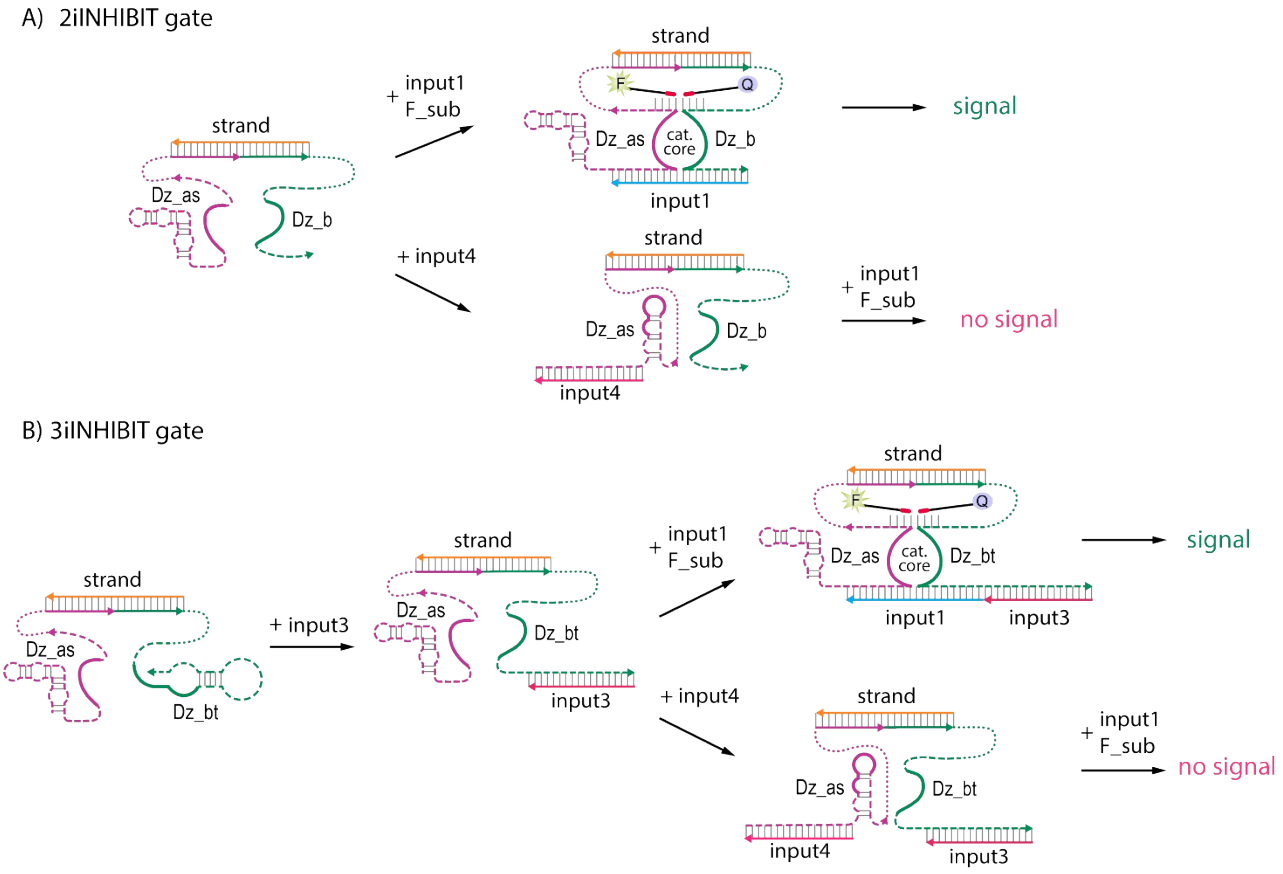

Figure S13. Schematic representation of mechanisms: A) 2iINHIBIT and B) 3iINHIBIT gates.

References

1 M. Zuker, *Nucleic Acids Res.*, 2003, **31**, 3406–3415.

2 V. S. Drozd, A. A. Eldeeb, D. M. Kolpashchikov and D. D. Nedorezova, *Nucleic Acid Ther.*, 2022, **32**, 412–420.

3 A. G. Gomes de Oliveira, M. V. Dubovichenko, A. A. ElDeeb, J. Wanjohi, S. Zablotskaya and D. M. Kolpashchikov, *Chembiochem*, 2021, **22**, 1750–1754.

4 C. Patra and A. A. ElDeeb, *ChemMedChem*, 2023, **18**, e202300040.